https://doi.org/10.1007/s41230-024-3064-3

Effect of electrical parameters and slag system on macrostructure of electroslag ingot

Bing-jie Wang, Yu Wang, Meng-jun Wang, Lei Zhao, Li-zhong Chang, and *Xiao-fang Shi

School of Metallurgy engineering, Anhui University of Technology, Ma'anshan 243002, Anhui, China

Abstract: To investigate the influence of electric parameters and slag system on the solidification quality of electroslag ingot during electroslag remelting, different power supply modes, current strengths and remelting slag systems were used to conduct electroslag remelting experiments on 304L austenitic stainless steel, and the macrostructure of electroslag ingots was analyzed. The results indicate that the depth of the metal pool decreases with the reduction of remelting frequency in the low frequency power supply mode. The effects of different power supply modes, such as low-frequency, direct current straight polarity (DCSP), and direct current reverse polarity (DCRP), on reducing the depth of the metal pool increase in that order. By reducing the remelting current strength in the same power supply mode, the depth of metal pool is reduced. When compared to the binary slag system of 70% CaF_2+30% Al_2O_3, the ternary slag system of 60% CaF_2+20% Al_2O_3+20% CaO is more effective in reducing the depth of the metal pool during remelting. Utilizing the 60% CaF_2+20% Al_2O_3+20% CaO ternary slag system results in a shallower and flatter metal pool, with columnar crystal growth occurring closer to the axial crystal. This effect is observed for both low frequency and direct current (DC) power supply modes.

Keywords: electroslag remelting; frequency; slag system; solidification quality

CLC numbers: TG142.1 **Document code:** A **Article ID:** 1672-6421(2024)01-044-07

1 Introduction

The solidification structure is crucial to the quality of steel. Defects such as porosity, shrinkage cavity, inclusion aggregation and segregation in steel are often formed during solidification [1-2]. In order to produce high-quality slabs, it is necessary to reduce composition segregation and avoid central shrinkage cavities [3-4]. Electroslag remelting is a key melting process with unique solidification conditions for the preparation of high-end special steels and alloys [5-7]. In the remelting process, the melting of the electrode and the crystallization of the molten metal are carried out simultaneously. The use of a water-cooled crystallizer with strong cooling capacities results in a relatively high cooling rate which inhibits the sufficient diffusion of elements in the solid and liquid phases, thus reducing component segregation. Additionally, it enhances axial crystallization tendencies, thereby improving the overall solidification quality of electroslag ingots [8-9].

Currently, the single-phase electroslag furnace with 50 Hz power supply is the most commonly used equipment for electroslag remelting. However, as the diameter of electroslag ingots and working currents continue to increase, the voltage drop across the short net increases proportionally, leading to an increase in reactive power during operation. This results that the power factor of the electroslag furnace's power supply system decreases, leading to substantial energy wastage and issues such as three-phase imbalance and harmonic pollution [10-11]. To address these issues, metallurgists use the low-frequency or direct current (DC) electroslag remelting as a means to overcome the limitations of power frequency remelting and improve energy efficiency. Researchers also have conducted extensive studies to investigate the impact of different frequency power supplies on metallurgical quality during remelting. Sibaki et al. [12] conducted numerical simulation research to investigate the effect of current frequency on the electroslag remelting process. They analyzed the influence of power frequencies, specifically 50 Hz and low frequency 0.2 Hz, on the remelting process. The results indicated that reducing the frequency can alter the distribution of Joule heat and electromagnetic force, resulting in a slight reduction in the depth of the metal pool during low-frequency electroslag remelting. Liang et al. [13] utilized MeltFlow software to study the effect of frequency on

***Xiao-fang Shi**

Female, born in 1978, Ph.D., Associate Professor. Research interests: Stainless steel metallurgy and electroslag remelting.

E-mail: shixiaofang602@163.com

Received: 2023-05-25; Accepted: 2023-08-23

solidification process parameters such as secondary dendrite spacing, local solidification time and Rayleigh value during electroslag remelting of GH4169 alloy. Research results showed that when the frequency was below 40 Hz, these parameters fluctuate significantly with the change of frequency, while, as the frequency is higher than 40 Hz, the changes of the three parameters with the change of frequency tend to slow down. Li et al. [14] used 3D finite element model (FEM) to analyze the distribution law of electromagnetic field when the power frequency was varied. Studies showed that when the remelting frequency changed from 10 Hz→20 Hz→30 Hz →40 Hz, the skin effect on the surface of the electrode and the ingot became more significant, and when the power supply frequency exceeded 40 Hz, eddy currents would be generated inside the electrode and the ingot.

Although some metallurgists have conducted research on low-frequency electroslag remelting technology, little attention has been given to the influence of current intensity and slag system under different power supply modes. Thus, based on previous research efforts, this study aims to investigate the impact of different remelting current strengths and remelting slag systems on the solidification quality of electroslag ingots. To achieve this, a self-designed frequency conversion equipment was used. The 304L austenitic stainless steel was used as the primary material and low-frequency (10 Hz, 5 Hz, 2 Hz) and DC supply modes were employed. The findings from this study are expected to offer valuable insights into understanding how these factors influence both the process and product quality.

2 Experimental

2.1 Experimental materials

Table 1 shows the main compositions of 304L austenitic stainless steel, which was used as the consumable electrode material in this experiment. The 304L austenitic stainless steels, obtained from Anhui Fukai Material Co., Ltd., were the continuous casting billets produced through the electric arc furnace (EAF)-argon oxygen decarburization (AOD)-ladle furnace (LF)-continuous casting (CC) process. These billets had a diameter of 280 mm. Subsequently, the continuous casting billets were forged into metal consumable electrodes with a diameter of 55 mm and a length of 850 mm. The slag used in the electroslag remelting process was 30% Al_2O_3+70% CaF_2 and 20% Al_2O_3+20% CaO+60% CaF_2, respectively, both weighing 1,200 g.

Table 1: Main compositions of 304L austenitic stainless steel (wt.%)

C	Si	Mn	P	S	Cr	Al	O	Fe
0.019	0.41	1.18	0.037	0.0025	18.27	0.010	0.0025	Bal.

2.2 Experimental equipment

The main parameters of the experimental electroslag furnace are as follows: a copper water-cooled crystallizer with an upper opening diameter of Φ_1=95 mm, a lower opening diameter of Φ_2=105 mm, and a height of h=250 mm. The transformer has a capacity of 100 kVA, with a high voltage terminal of 380 V and a low voltage terminal ranging from 28–40 V. It is designed to handle a maximum current of 2,500 A. The remelting process adopts manual control of the variable speed motor, and the up and down movement of the consumable electrode is realized by the rotating the worm gear. The experimental equipment is schematically shown in Fig. 1. The main circuit of the frequency conversion unit in a thyristor rectifier power supply consists of two single-phase bridge-type thyristor-controlled rectifier circuits connected in antiparallel. The two single-phase bridge-type rectifier circuits are controlled to conduct alternately by the control circuit's trigger, thereby producing an alternating output current (AC). The output is positive when the positive bridge is turned on and negative when the negative bridge is turned on.

The main circuit of frequency conversion unit is composed of two reverse parallel single-phase bridge thyristor rectifiers. By controlling the duration of the alternating conduction of the two rectifier circuits, the output frequency can be adjusted between 0 and 10 Hz, allowing for both low-frequency and DC output. Additionally, by adjusting the conduction angle of the thyristor, the output voltage can be continuously adjusted between 0 and the transformer's output voltage. The output of the frequency conversion unit is connected to a consumable electrode and a cooled copper baseplate. During the remelting process, the voltage and frequency are fixed, while the current can be adjusted by manually controlling the speed of the consumable electrode.

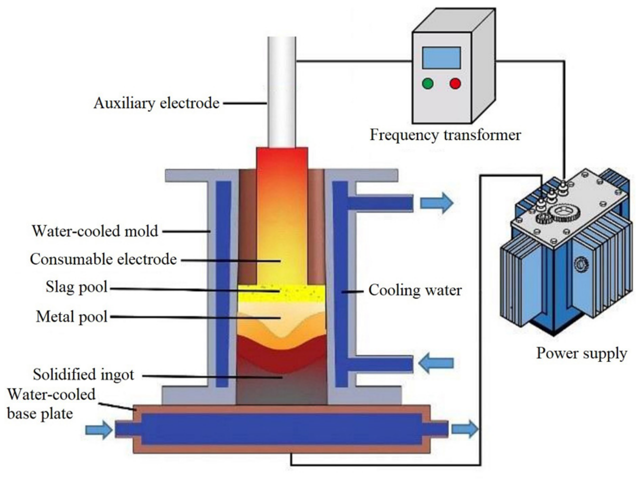

Fig. 1: Experimental device of variable frequency power supply electroslag furnace

2.3 Experimental process

A total of 1,200 g of slag was used for the remelting process. The slag was evenly mixed and put into a graphite crucible. Then, the crucible was heated in a molybdenum disilicide high-temperature tube furnace to above 1,650 °C, ensuring that the slag was completely melted. The diameters of metal consumable electrode and mold were 55 mm and 100 mm, respectively, and the pressure of the cooling water used to cool the crystallizer was 0.2–0.3 MPa. Before remelting, all iron oxide scale on the surface of electrode was removed from the electrode surface. The frequency conversion unit was adjusted to the specified frequency. The molten slag was then rapidly poured into the crystallizer, followed by the descent of the consumable electrode and the commencement of remelting. Subsequently, the current was gradually increased until reaching the target value, marking the transition into normal remelting stage. Once the electroslag ingot reached the predetermined height, the power was shut off. After the slag cap had fully solidified, it was removed to allow for easier sample cutting in subsequent steps.

Finally, the electroslag ingot with a height of 200 mm was obtained. The top and bottom of the electroslag ingots were removed by 30 mm using a sawing machine. The upper part of the remaining electroslag ingot with a height of 140 mm was then cross-sectioned to obtain a circular section with a thickness of 30 mm. Finally, the remaining electroslag ingots with a height of 110 mm were further longitudinally sectioned, resulting in two semi-cylindrical electroslag ingots. The longitudinal and cross sections were ground with sandpaper ranging from #80 to #800. The samples were then corroded at 50–70 °C for 10–30 min. Subsequently, the samples were placed in a saturated bicarbonate scrub in sodium aqueous solution to remove the acid film attached to the surface, and then washed with dilute hydrochloric acid to neutralize the sodium bicarbonate attached to the surface. Any stains attached to the surface of the samples were rinsed with 99.7% anhydrous ethanol. Finally, the surface of the sample was dried with a hair dryer.

To investigate the impact of various parameters and slag systems on electroslag remelting, twelve sets of experiments were designed with different parameter combinations. The experimental schemes are shown in Table 2.

Table 2: Experimental schemes with different parameter combinations

Experimental schemes	Power frequency (Hz)	Remelting voltage (V)	Remelting current (A)	Slag system
D1	10			
D2	5			
D3	2	20	1,400	30% Al_2O_3+70% CaF_2
D4	DCSP			
D5	DCRP			
D6	2	28	1,800	
D7	2	20	1,000	30% Al_2O_3+70% CaF_2
D8	DCSP	28	1,800	
D9	DCRP	28	1,800	
D10	2			
D11	DCSP	28	1,800	20% Al_2O_3+20% CaO+60% CaF_2
D12	DCRP			

3 Results and analysis

3.1 Effect of different power frequencies on solidification structure of electroslag ingot

Figure 2 shows that in the low-frequency power supply mode, the angle between the temperature gradient direction and the axial direction on the longitudinal section decreases gradually as the frequency decreases from 10 Hz to 5 Hz and 2 Hz. As a consequence, columnar crystals tend to grow in the axial direction, resulting in a shallower depth of the metal pool. Additionally, there is an increased presence of equiaxed crystal regions on the cross section, as shown in Figs. 2(a) to (c). When DCSP and DCRP modes were utilized, the angles between the temperature gradient direction and the axial direction are approximately 12.5° and 8.5°, respectively. As shown in Figs. 2(d) and (e), the depth of both metal pools is shallow. Therefore, in the low-frequency power supply mode, changing the remelting frequency reasonably can effectively reduce the depth of the remelting pool and improve the

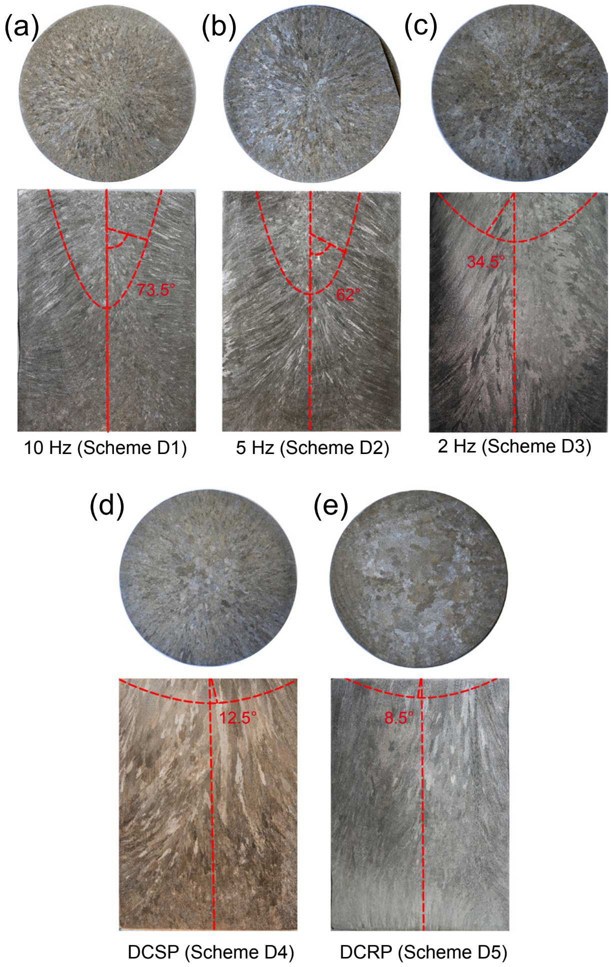

Fig. 2: Macrostructures of transversal and longitudinal sections of electroslag ingot under different power supply modes

solidification quality [15]. In comparison to the low-frequency power supply mode, the DC power supply mode produces a shallower metal pool, with the shallowest pool occurring when using DC reverse connection for remelting.

3.2 Effect of different current intensities on solidification structure of electroslag ingot

Figure 3 shows the macrostructures of the ingots prepared with different remelting currents (1,000–1,800 A) in low-frequency power supply mode (2 Hz) and DC power supply mode. It can be seen that either in low-frequency power supply mode or DCSP, DCRP, decreasing the remelting current intensity leads to a gradual reduction in the angle between the temperature gradient direction and the axial direction. This results that the columnar crystals gradually tend to grow axially, the depth of the metal pool gradually becomes shallower, and the equiaxed crystal region correspondingly becomes larger. When utilizing the DCRP mode with a current intensity of 1,400 A, there is a minimum angle of approximately 8.5° between the temperature gradient direction and axial direction. Additionally, the metal pool reaches its shallowest depth. Therefore, by appropriately reducing the intensity of remelting current, it is possible to promote axial growth of the crystals in the solidified structure and decrease the depth of the metal pool.

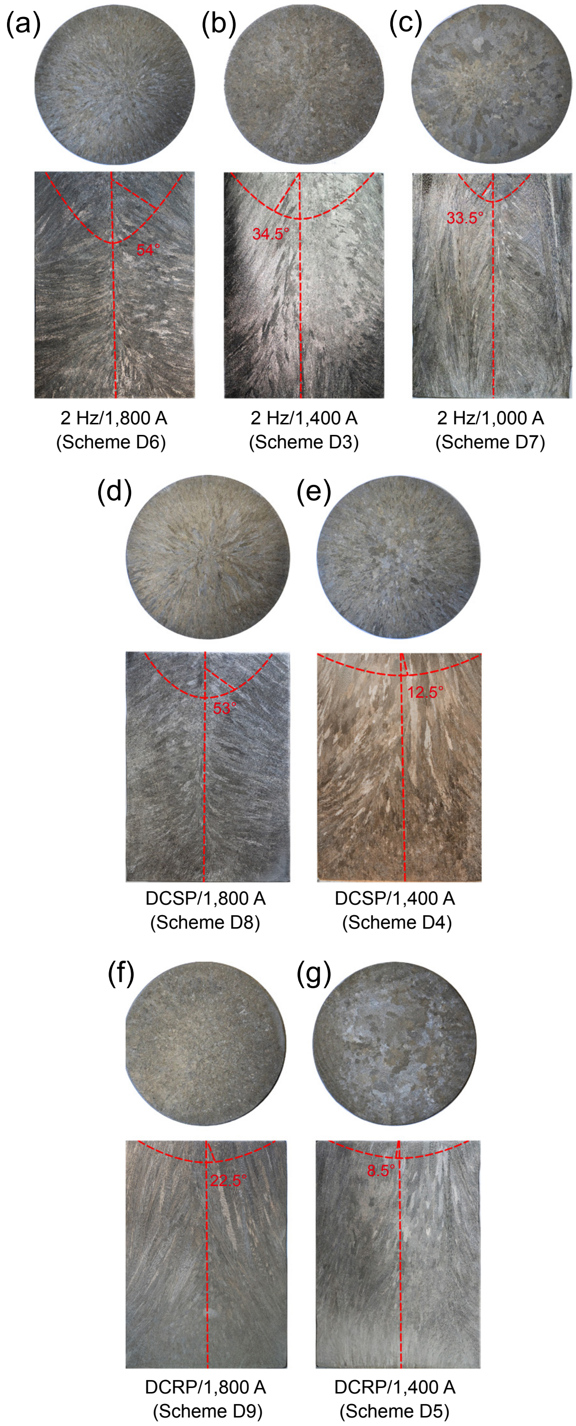

Fig. 3: Macrostructures of transversal and longitudinal sections of electroslag ingot under different current intensities

3.3 Effect of different slag systems on solidification structure of electroslag ingot

Figure 4 shows the macrostructure of the ingot under low-frequency power supply mode (2 Hz) and DC power supply mode remelted by different slag systems. It can be seen from Fig. 4 that when using the binary slag of 30% Al_2O_3+70% CaF_2 for remelting at a low power frequency of 2 Hz, the angle between the temperature gradient direction and axial direction is approximately 54°. However, when the ternary slag system of 20% Al_2O_3+20% CaO+60% CaF_2 is used, this angle decreases

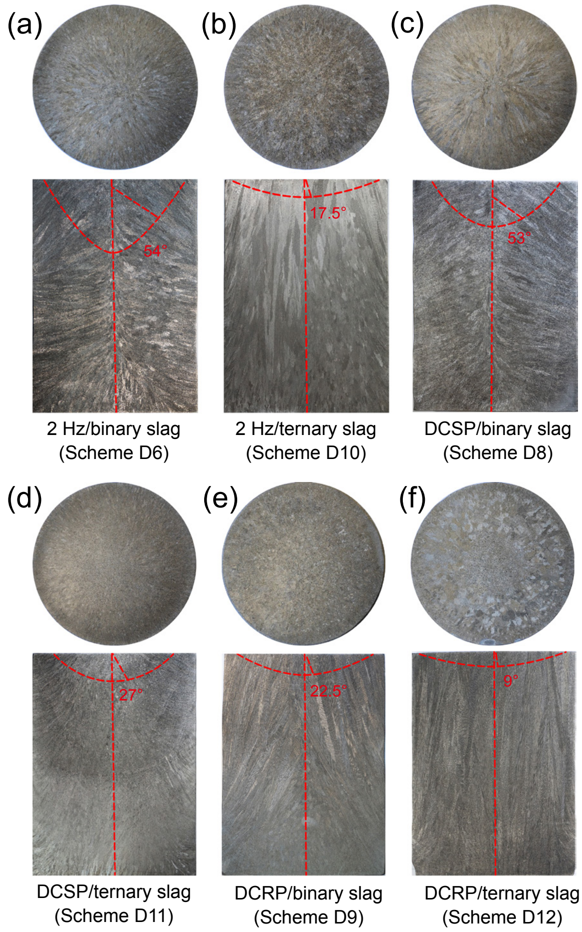

Fig. 4: Macrostructures in transversal and longitudinal sections of electroslag ingot under different slag systems

to about 17.5° along with a shallower molten pool, indicating a closer trend towards axial growth. When employing the DCSP power supply mode for remelting, using the ternary slag system results in a smaller angle between the temperature gradient direction and axial direction (27°) compared to the binary slag system (53°). The columnar crystal size is smaller, and axial growth is more pronounced, resulting in a shallower metal pool. Similarly, under the DCRP power supply mode, using a ternary slag system results in a smaller angle between the temperature gradient direction and axial direction (9°) compared to the binary slag system (22.5°). This results in a shallower metal pool. This indicates that a ternary slag system promotes axial growth and reduces the depth of the metal pool, regardless of whether it is used in low frequency, DCSP, or DCRP mode.

4 Discussion

The results from the aforementioned study show that the solidification microstructure of electroslag ingot undergoes significant changes during electroslag remelting, depending on the power supply modes, current intensity, and slag systems used. During the electroslag remelting process, a circuit is formed among the self-consuming electrode, slag pool, metal pool, ingot and water-cooled base plate via a short network [16]. When a remelting current is applied, it generates a magnetic field in the liquid slag pool. The electric and magnetic fields interact, creating an electromagnetic force that drives the slag and metal pools, resulting in a more uniform temperature in the slag pool [17-18]. The electromagnetic force (F) is represented in Eq. (1):

$$F=\vec{J}\times\vec{B}=\frac{\left(\vec{B}\cdot V\right)\cdot\vec{B}}{\mu}-\frac{V\cdot\vec{B}^2}{2\cdot\mu}\infty\frac{1}{\sqrt{\pi\cdot\mu\cdot f\cdot\sigma}}\cdot D^{-1} \quad (1)$$

where $\vec{B}$ is the magnetic flux density, T; V is the flow rate of liquid metal or slag, m·s^{-1}; μ is the magnetic permeability, F·m^{-1}; D is the inner diameter of crystallizer, m; f is the power frequency, Hz; and σ is the electrical conductivity, S·m^{-1}. $\frac{\left(\vec{B}\cdot V\right)\cdot\vec{B}}{\mu}$ is the rotational component driving the melt flow; $\frac{V\cdot\vec{B}^2}{2\cdot\mu}$ is the spinless component acting on the surface of the melt, i.e. the electromagnetic pressure.

It can be seen from Eq. (1) that the electromagnetic force of the remelting system and AC power supply frequency is inversely related: the lower the frequency, the greater the electromagnetic force. When the electromagnetic force increases, it drives the movement of the metal and slag pools. The movement causes the high-temperature region at the center of the slag pool to move outward, resulting in a more uniform temperature distribution at the slag-metal interface and throughout the metal pool. This is beneficial for heat dissipation through the water-cooled mold, which reduces the depth of the metal pool and promotes the growth of columnar crystal, leading to an overall improvement in solidification quality.

Figure 5 shows the current distribution in the slag pool when the DC power supply mode is adopted [19]. When DCSP is adopted, the positive pole of the power supply connects to the water-cooled base plate. The current enters the slag pool from the water-cooled base plate and converges at the end of

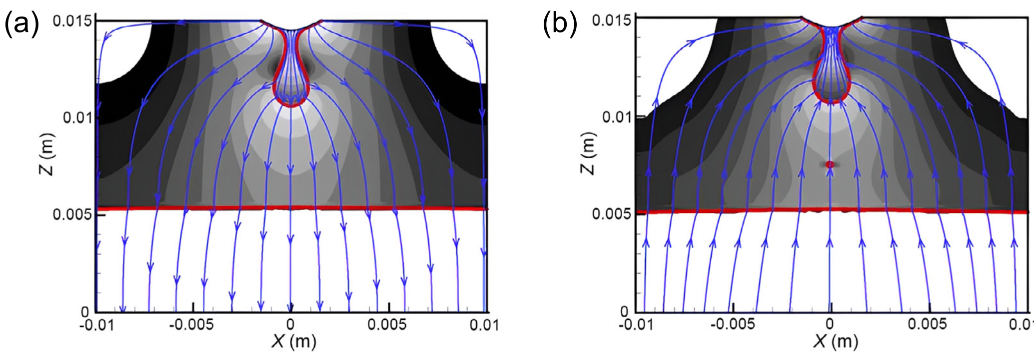

Fig. 5: Electric current streamlines: (a) DCRP; and (b) DCSP

the consumable electrode (melt droplet) before returning to the negative pole of the transformer. In contrast, when DCRP is adopted, the self-consumable electrode connects to the positive pole of the power supply. In this case, the current enters the slag pool through the electrode end (melt droplet) before returning to the negative pole of the power supply. Therefore, the DCSP mode results in a lower current density outside the slag pool and a higher current density at the droplet compared to the DCRP mode. This difference in current density distribution leads to a higher Lorentz force outside the slag pool during DCRP remelting. Conversely, during DCSP remelting, the Lorentz force inside the droplet is higher [18]. As a result, when using the DCSP power supply mode, the droplet falls faster and the high-temperature area is mainly distributed in the centre of the slag pool, which is not conducive to carrying away internal heat by the water-cooled crystallizer, resulting in a deeper metal pool. On the contrary, when using the DCRP, the Lorentz force outside the slag pool is greater, which causes more vigorous stirring of the metal and slag pools, so that the high temperature area in the centre of the slag pool is shifted outward, prompting the slag-steel interface and the temperature of all parts of the metal pool to be more uniform, thus reducing the depth of the metal pool. In this experiment, under the premise of the same current strength and slag system, the DCRP method produces the shallowest metal pool depth.

The constant magnetic field generated by DC maintains its magnitude and direction, while the magnitude and direction of the electromagnetic force generated by AC vary based on the frequency of the power supply. Due to the phenomenon of partial cancellation of the electromagnetic force in AC power supply, the magnetic field generated by the DC power supply is more powerful. Therefore, as the other remelting parameters keep constant, the metal pool depth is shallower by DC than that by AC power supply.

The change of current intensity also has a great influence on the shape of the metal pool. The macrostructure of electroslag remelting ingots is strongly influenced by the shape of the metal pool, which is closely related to the distribution of heat flow resulting from the magnitude and path of the remelting current. Under the premise that the power frequency is constant, the remelting current has a linear relationship with the depth of the metal pool as follows [20]:

$$h_{\text{liquid-phase}} = 0.00244I - 336.7 \tag{2}$$

$$h_{\text{solid-phase}} = 0.0371I - 689.8 \tag{3}$$

where $h_{\text{liquid-phase}}$ is the liquidus line depth, mm; $h_{\text{solid-phase}}$ is the solidus line depth, mm; and I is the remelting current, A.

It can be seen from Eqs. (2) and (3) that as the current increases, the metal pool becomes deeper and the distance between the solid-liquid two-phase region increases.

Different slag systems have a significant impact on the depth of the metal pool. When power frequency, remelting current, and remelting voltage remain constant, the insertion depth of the consumable electrode in the slag pool will vary with changes in slag conductivity. This change in insertion depth directly affects the depth of the metal pool [21-22].

The relationship between the conductivity (k, $\Omega^{-1}\cdot cm^{-1}$) of the slag and its composition can be derived from Eq. (4) [23-24]:

$$k = 100\exp\left(1.911-1.38N-5.69N^2\right) + 0.39\left(T-1973\right) \tag{4}$$

where $N=N_{Al_2O_3}+0.2\times N_{CaO}+0.75\times N_{SiO_2}+0.5\times(N_{SiO_2}+N_{ZrO_2})$; $N_{Al_2O_3}$, N_{CaO}, N_{SiO_2}, N_{TiO_2}, N_{ZrO_2} are the corresponding molar fraction of each component, respectively; T is the temperature between 1,823–2,053 K.

The electrical conductivity calculation results of the binary and ternary slag systems used in this experiment at 1,650–1,750 °C are shown in Table 3.

It can be seen from the calculation results in Table 3 that when the Al_2O_3 content in the slag system decreases and the CaO content increases, the electrical conductivity of the slag system increases. In order to ensure the same remelting current and voltage when different slag systems are used, the electrode insertion depth into the slag pool must be adjusted. The relationship between the insertion depth of the electrode in the slag pool and the slag conductivity can be expressed by Eq. (5) [15]:

$$H_1 = R_S \cdot r_s \cdot S_E; \qquad H_3 = H_2 - H_1 \tag{5}$$

where H_1 is the distance from the electrode tip to the metal pool, cm; R_S is the slag pool resistance, Ω; r_s is the slag conductivity, $S\cdot cm^{-1}$; S_E is the conductive area of electrodes, cm^2; H_2 is the slag pool depth, cm; H_3 is the insertion depth of the electrode in the slag pool, cm.

According to Eq. (5), when the diameter of the consumable electrode and the resistance of the slag pool remains constant, an increase in conductivity due to changes in the slag system will result in an increase in H_1. This means that when transitioning from a binary slag system to a ternary slag system, the distance between the consumable electrode and the metal pool will increase, causing a reduction in the depth of the electrode head buried in the slag. As a result, the high-temperature zone of the slag pool will shift upward, the temperature of the metal pool will decrease, and the depth of the metal pool will become shallower, thus further promoting the development of axial crystallization.

Table 3: Conductivity ($\Omega^{-1}\cdot cm^{-1}$) of different slag systems at different temperatures

Slag system	1,650 °C	1,700 °C	1,750 °C
30% Al_2O_3+70% CaF_2	3.20	3.40	3.59
20% Al_2O_3+20% CaO+60% CaF_2	3.85	4.05	4.24

5 Conclusions

(1) When the slag system and remelting current are kept constant, decreasing the frequency (10 Hz, 5 Hz, 2 Hz, and 0 Hz) results in a decrease in the depth of the metal pool. This can be attributed to an increase in electromagnetic force caused by the

lower remelting frequency in low-frequency power supply mode. The increased electromagnetic force promotes outward movement of the high-temperature area at the center of the slag pool, leading to a more uniform temperature distribution at both the slag-metal interface and various parts within the metal pool. Finally, this leads to a reduction in the depth of the metal pool.

(2) When the slag system and the remelting current remain constant, the metal pool becomes relatively shallow when the DC power supply mode is used compared to low frequency mode, and the metal pool depth is the shallowest under the DCRP remelting mode. Under the premise of a fixed power frequency (low frequency or DC), increasing the current intensity results in an increase in the heat capacity of the slag pool and the depth of the metal pool. This is consistent with the traditional electroslag remelting theory.

(3) In contrast to the 30% Al_2O_3+70% CaF_2 binary slag system, the metal pool exhibits a shallow and flat distribution of columnar crystals that are close to axial crystallization when remelts with the 20% Al_2O_3+20% CaO+60% CaF_2 ternary slag system. This can be attributed to the higher conductivity of the ternary slag system, which results in a shallower insertion depth and an upward movement of the high temperature zone of the slag pool under the same voltage and current conditions. As a result, the temperature of the slag pool becomes more uniform, leading to a shallower metal pool.

Acknowledgments

This work was financially supported by the National Natural Science Foundation of China (Grant Nos. 52074002, 52174289) and Natural Science Foundation of Anhui Province (Grant No. 2208085J37).

Conflict of interest

The authors declare that they have no known competing financial interests or personal relationships that could have appeared to influence the work reported in this paper.

References

[1] Chu J H, Zhang L Q, Yang J, et al. Characterization of precipitation, evolution, and growth of MnS inclusions in medium/high manganese steel during solidification process. Materials Characterization, 2022, 194: 112430.

[2] Kang C P, Liu F B, Jiang Z H, et al. Effect of nitrogen content on solidification behaviors and morphological characteristics of the precipitates in 55Cr17Mo1VN plastic die steel. Materials Characterization, 2022, 194: 112367.

[3] Wang Y D. Study on the effect of electromagnetic stirring on the macrosegregation of steel continuous casting blooms. Doctoral Dissertation, University of Science and Technology Beijing, 2022: 1–2. (In Chinese)

[4] Jia L J. Analysis and control of segregation in high carbon steel billet casts. Metallurgy and Materials, 2022, 42(2): 121–122.

[5] Li B K, Huang X C, Liu Z Q, et al. Characteristics and evolution of advanced modern electroslag remelting technologies. Iron & Steel, 2022, 57(6): 1–11. (In Chinese)

[6] Lv B, Li Z Q, Yang Z Y, et al. Effect of ESR process on the solidification structure of GCr15 bearing steel. Materials Reports, 2021, 35(24): 134–141. (In Chinese)

[7] Wang Q, Wang F, He Z, et al. Development of numerical simulation in electroslag metallurgy. Journal of Iron and Steel Research, 2021, 33(8): 681–694. (In Chinese)

[8] Shi X F, Xu T, Chang L Z. Effect of electromagnetic stirring on metallurgical quality of GCr15 electroslag ingot. China Foundry, 2022, 19(1): 46–54.

[9] Zheng D L, Ma G J, Zhang X, et al. Evolution of MnS and MgO·Al_2O_3 inclusions in AISI M35 steel during electroslag remelting. Journal of Iron and Steel Research International, 2021, 28(12): 1605–1616.

[10] Lv P. Key technology of large-tonnage electroslag furnace low frequency power supply. Master's Dissertation, Xi'an Shiyou University, 2017. (In Chinese)

[11] Yu K, Yu A S, Yang X J. Effects of low frequency electroslag remelting on microstructure and properties of No. 8367 austenitic stainless steel. Special Casting & Nonferrous Alloys, 2019, 39(2): 133–136. (In Chinese)

[12] Sibaki E K, Kharicha A, Wu M, et al. A Numerical study on the influence of the frequency of the applied AC current on the electroslag remelting process. In: Proceedings of the 2013 International Symposium on Liquid Metal Processing & Casting. Cham: The Minerals. TMS, 2016: 13–19.

[13] Liang Q, Chen X C, Ren H, et al. Effects of power frequency on solidification process parameters of GH4169 alloy in electroslag remelting process. Special Casting & Nonferrous Alloys, 2012, 32(4): 302–306. (In Chinese)

[14] Li B K, Wang F, Tsukihashi F. Current, magnetic field and joule heating in electroslag remelting processes. ISIJ International, 2012, 52(7): 1289–1295.

[15] Li Z B. Electroslag metallurgy theory and practice. Beijing: Metallurgical Industry Press, 2010. (In Chinese)

[16] Ren N, Wang Q, Li B K. Numerical simulation of the electroslag remelting process. In: Proceedings of the 8th National Conferance on Energy and Thermal Engineering. Edited by Energy and Thermal Engineering Branch of China Metal Society, Dalian, Liaoning, China, 2015: 171–175.

[17] Zhu C L, Zhang L F, Su Y L, et al. Effect of electromagnetic stirring on inclusions in 304 stainless steel electroslag ingot. Journal of Iron and Steel Research, 2022, 34(9): 933–943. (In Chinese)

[18] Qi W T, Guo Y F, Ma C K, et al. Multi-stage enhanced removal of inclusions during electroslag remelting process by a static magnetic field. Steel Research International, 2022, 93(10): 2200273.

[19] Wang Q, Liu Y, Wang F, et al. Numerical study on the effect of electrode polarity on desulfurization in direct current electroslag remelting process. Metallurgical and Materials Transactions, 2017, 48(5): 2649–2663.

[20] Duan J C, Dong Y W, Jiang Z H, et al. Numerical simulation study of operate parameters effect on ERS process. Jiangxi Metalllurgy, 2014, 34(1): 5–8, 12. (In Chinese)

[21] Chen X, Liu F B, Li X, et al. A numerical simulation for effect of technological parameters on hollow ingot solidification in electroslag remelting process. Journal of Materials and Metallurgy, 2015, 14(2): 100–106. (In Chinese)

[22] Liu S J. Electrode insert into depth for electrical dregs weight rong importance in ESR course. Journal of Materials and Metallurgy, 2011, 10(S1): 73–76. (In Chinese)

[23] Dong Y W, Jiang Z H, Li H B, et al. Conductivity calculation of slag containing fluoride used for electroslag metallurgy. Journal of Materials and Metallurgy, 2012, 11(4): 274–277. (In Chinese)

[24] Dong Y W. Mathematical modeling of solidification during electroslag remelting process and development of new slags. Doctoral Dissertation, Northeastern University, 2008: 44–45. (In Chinese)